Erbium-doped glass nanoparticle embedded polymer thin films using femtosecond pulsed laser deposition

ERIC KUMI BARIMAH,[1,*] MARCIN W. ZIARKO,[2] NIKOLAOS BAMIEDAKIS,[2] IAN H. WHITE,[2] RICHARD V. PENTY,[2] AND GIN JOSE[1]

[1]*School of Chemical and Process Engineering, University of Leeds, Clarendon Road, Leeds LS2 9JT, UK*
[2]*Centre for Photonic Systems, Department of Engineering, University of Cambridge, 9 J. J. Thomson Ave, Cambridge CB3 0FA, UK*
*preeku@leeds.ac.uk

Abstract: Polymer materials doped with rare-earth ions are promising candidates for the formation of low-cost integrated optical amplifiers. However, there are significant technical challenges associated with the integration of these dissimilar materials and the formation of high-quality Er-doped polymer films. In this paper, therefore, we present for the first time the fabrication of polymer thin layers modified with erbium-doped sodium zinc tellurite (Er-TZN) glass nanoparticles (NPs) using femtosecond (fs) pulsed laser deposition (PLD) and the characterisation of their basic properties. The surface morphology and the compositional and structural characteristics of the samples produced with this method are evaluated using scanning and transmission electron microscopy (SEM and TEM) and X-ray diffraction (XRD), while photoluminescence (PL) measurements are carried out at room temperature under a 980 nm laser diode excitation. The studies indicate that the Er-doped TZN NPs are successfully integrated in the polymer layers. The obtained average NP size is measured to be in the range of 12 to 21 nm depending on the fabrication parameters, while broad PL emission at 1534 nm that corresponds to the $^4I_{13/2} \rightarrow {}^4I_{15/2}$ transition of Er^{3+} is observed from the samples. The full-width at half-maximum (FWHM) of the PL spectra is found to be ~39 nm while the fluorescence lifetime is measured to be in the range of 3.52 to 4.18 ms. The obtained results clearly demonstrate the potential to efficiently dope polymer layers with glass NPs using fs-PLD and is a first step towards the successful formation of hybrid polymer-glass waveguide amplifiers.

References and links

1. Z. Zhao, G. Jose, P. Steenson, N. Bamiedakis, R. V. Penty, I. H. White, and A. Jha, "Tellurite glass thin films on silica and polymer using UV (193 nm) pulsed laser ablation," J. Phys. D Appl. Phys. **44**(9), 095501 (2011).
2. C. E. Brunchi, A. Filimon, M. Cazacu, and S. Ioan, "Properties of some poly(siloxane)s for optical applications," High Perform. Polym. **21**(1), 31–47 (2009).
3. V. Prajzler, P. R. Mastera, and P. Nekvindova, "Properties of siloxane based optical waveguides deposited on transparent paper and foil," Wuxiandian Gongcheng **25**(2), 230 (2016).
4. H. Ma, A. K.-Y. Jen, and L. R. Dalton, "Polymer-based optical waveguides: materials, processing, and device," Adv. Mater. **14**(19), 1339–1365 (2002).
5. R. S. E. John, C. M. Amb, B. W. Swatowski, W. K. Weidner, M. Halter, T. Lamprecht, and F. Betschon, "Thermally stable, low loss optical silicones: a key enabler for electro-optical printed circuit boards," J. Lightw. Tech. **33**(4), 814–819 (2015).
6. E. Zgraggen, I. M. Soganci, F. Horst, A. La Porta, R. Dangel, B. J. Offrein, S. A. Snow, J. K. Young, B. W. Swatowski, C. M. Amb, O. Scholder, R. Broennimann, U. Sennhauser, and G.-L. Bona, "Laser direct writing of single-mode polysiloxane optical waveguides and devices," J. Lightw. Tech. **32**, 814 (2015).

7. J. C. Dingeldein, K. A. Walczak, B. W. Swatowski, C. R. Friedrich, C. T. Middlebrook, and M. C. Roggemann, "Process characterization for direct dispense fabrication of polymer optical multi-mode waveguides," J. Micromech. Microeng. **23**(7), 075015 (2013).
8. R. Dangel, F. Horst, D. Jubin, N. Meier, J. Weiss, B. J. Offrein, B. W. Swatowski, C. M. Amb, D. J. DeShazer, and W. K. Weidner, "Development of versatile polymer waveguide flex technology for use in optical interconnectsm," J. Lightw. Tech. **31**(24), 3915–3926 (2013).
9. N. Bamiedakis, A. Hashim, R. V. Penty, and I. H. White, "A 40 Gb/s optical bus for optical backplane interconnections," J. Lightw. Tech. **32**(8), 1526–1537 (2014).
10. J. Beals, N. Bamiedakis, A. Wonfor, R. Penty, I. White, J. DeGroot, K. Hueston, T. Clapp, and M. Glick, "A terabit capacity passive polymer optical backplane based on a novel meshed waveguide architecture," Appl. Phys., A Mater. Sci. Process. **95**(4), 983–988 (2009).
11. R. C. A. Pitwon, W. Kai, J. Graham-Jones, I. Papakonstantinou, H. Baghsiahi, B. J. Offrein, R. Dangel, D. Milward, and D. R. Selviah, "FirstLight: pluggable optical interconnect technologies for polymeric electro-optical printed circuit boards in data centers," J. Lightw. Tech. **30**(21), 3316–3329 (2012).
12. M. Immonen, R. Zhang, M. Press, H. Tang, W. Lei, J. Wu, H. J. Yan, L. X. Zhu, and M. Serbay, "End-to-end optical 25Gb/s link demonstrator with embedded waveguides, 90° out-of-plane connector and on-board optical transceivers," in *42nd European Conference on Optical Communication (ECOC)* (2016). 1–3.
13. G. A. Kumar, C. W. Chen, R. Riman, S. Chen, D. Smith, and J. Ballato, "Optical properties of a transparent CaF$_2$:Er^{3+} fluoropolymer nanocomposite," Appl. Phys. Lett. **86**(24), 241105 (2005).
14. L. H. Slooff, A. Polman, M. P. Oude Wolbers, F. C. J. M. V. Veggel, D. N. Reinhoudt, and J. W. Hofstraat, "Optical properties of erbium-doped organic polydentate cage complexes," J. Appl. Phys. **83**(1), 497–503 (1998).
15. M. Zhang, W. Zhang, F. Wang, D. Zhao, C. Qu, X. Wang, Y. Yi, E. Cassan, and D. Zhang, "High-gain polymer optical waveguide amplifiers based on core-shell NaYF$_4$/NaLuF$_4$: Yb^{3+}, Er^{3+} NPs-PMMA covalent-linking nanocomposites," Sci. Rep. **6**(1), 36729 (2016).
16. X. Zhai, J. Li, S. Liu, X. Liu, D. Zhao, F. Wang, D. Zhang, G. Qin, and W. Qin, "Enhancement of 1.53 μm emission band in NaYF$_4$:Er^{3+}·Yb^{3+}·Ce^{3+} nanocrystals for polymer-based optical waveguide amplifiers," Opt. Mater. Express **3**(2), 270 (2013).
17. T. Kakkar, N. Bamiedakis, T. T. Fernandez, Z. Zhao, M. Irannejad, P. Steenson, A. Jha, R. Penty, I. White, and G. Jose, "Glass–polymer superlattice for integrated optics," Opt. Eng. **53**(7), 071818 (2014).
18. S. Ghatrehsamani and G. E. Town, "Optical gain in polymer composite materials with P$_2$O$_2$: Er^{3+}/Yb^{3+}- codoped nanoparticles," J. Quantum Electronics **53**(2), 7000705 (2017).
19. Q. Xiang, Y. Zhou, Y. L. Lam, Y. C. Chan, and C. H. Kam, "Deposition and characterization of Er^{3+} doped, A1 co-doped sol-gel silica films on SOS," Ferroelectrics **230**(1), 55–60 (1999).
20. T. Yada, T. Maejima, MasaruAoki, and M. Umesaki, "Thin-film formation by spin coating: characteristics of a positive photoresist," Jpn. J. Appl. Phys. **3**(1), 6279–6284 (1995).
21. S. C. Hamm, R. Shankaran, V. Korampally, S. Bok, S. Praharaj, G. A. Baker, J. D. Robertson, B. D. Lee, S. Sengupta, K. Gangopadhyay, and S. Gangopadhyay, "Sputter-deposition of silver nanoparticles into ionic liquid as a sacrificial reservoir in antimicrobial organosilicate nanocomposite coatings," ACS Appl. Mater. Interfaces **4**(1), 178–184 (2012).
22. S. Kar, S. Logad, O. P. Choudhary, C. Debnath, S. Verma, and K. S. Bartwal, "Preparation of lithium niobate nanoparticles by high energy ball milling and their characterization," J. Mater. Sci. **1**(2), 18–24 (2013).
23. E. Rebollar, S. Gaspard, M. Oujja, M. M. Villavieja, T. Corrales, P. Bosch, S. Georgiou, and M. Castillejo, "Pulsed laser deposition of polymers doped with fluorescent molecular sensors," Appl. Phys., A Mater. Sci. Process. **84**(1-2), 171–180 (2006).
24. R. A. Ganeev, U. Chakravarty, P. A. Naik, H. Srivastava, C. Mukherjee, M. K. Tiwari, R. V. Nandedkar, and P. D. Gupta, "Pulsed laser deposition of metal films and nanoparticles in vacuum using subnanosecond laser pulses," Appl. Opt. **46**(8), 1205–1210 (2007).
25. S. Eliezer, N. Eliaz, E. Grossman, D. Fisher, I. Gouzman, Z. Henis, S. Pecker, Y. Horovitz, M. Fraenkel, S. Maman, and Y. Lereah, "Synthesis of nanoparticles with femtosecond laser pulses," Phys. Rev. B **69**(14), 144119 (2004).
26. R. G. Nikov, A. O. Dikovska, N. N. Nedyalkov, G. V. Avdeev, and P. A. Atanasov, "Au nanostructure fabrication by pulsed laser deposition in open air: Influence of the deposition geometry," Beilstein J. Nanotechnol. **8**, 2438–2445 (2017).
27. I. Mirza, G. O'Connell, J. J. Wang, J. G. Lunney, "Comparison of nanosecond and femtosecond pulsed laser deposition of silver nanoparticles films," Nanotechnology **25**, 265301 (2014).
28. J. Chandrappan, M. Murray, P. Petrik, E. Agocs, Z. Zolnai, A. Tempez, S. Legendre, D. P. Steenson, A. Jha, and G. Jose, "Doping silica beyond limits with laser plasma for active photonic materials," Opt. Mater. Express **5**(12), 2849–2861 (2015).
29. J. W. Jeon, S. Yoon, H. W. Choi, J. Kim, D. Farson, S. -H. Cho, "The effect of laser pulse widths on laser-Ag nanoparticle interaction: femto- to-nanosecond lasers," Appl. Sci. **8**, 112–120 (2018).
30. M. Boutinguiza, M. Meixus, J. Del Val, A. Riverio, R. Comesana, F. Lusquinos, and J. Pou, "Synthesis and characterization of Pd nanoparticles by laser ablation in water using nanosecond laser," Phys. Procedia **83**, 36–45 (2016).

31. K. Vu and S. Madden, "Tellurium dioxide Erbium doped planar rib waveguide amplifiers with net gain and 2.8 dB/cm internal gain," Opt. Express **18**(18), 19192–19200 (2010).
32. S. Sakida, T. Nanba, and Y. Miura, "Optical properties of Er^{3+}-doped tungsten tellurite glass waveguides by Ag+-Na+ ion-exchange," Opt. Mater. **30**(4), 586–593 (2007).
33. V. A. G. Rivera, E. F. Chillcce, E. Rodriguez, C. L. Cesar, and L. C. Barbosa, "Planar waveguides by ion exchange in Er^{3+}-doped tellurite glass," J. Non-Cryst. Solids **352**(5), 363–367 (2006).
34. H. Liu, Z. Huang, J. Huang, S. Xu, M. Fang, Y. G. Liu, X. Wu, and S. Zhang, "Morphology controlling method for amorphous silica nanoparticles and jellyfish-like nanowires and their luminescence properties," Sci. Rep. **6**(1), 22459 (2016).
35. V. Koubassov, J. F. Laprise, F. Theberge, E. Forster, R. Sauerbrey, B. Muller, U. Glatzel, and S. L. Chin, "Ultrafast laser-induced melting of glass," Appl. Phys., A Mater. Sci. Process. **79**(3), 499–505 (2004).
36. S. M. Sidel, F. A. Santos, V. O. Gordo, E. Idalgo, A. A. Monteiro, J. C. S. Moraes, and K. Yukimitu, "Avrami exponent of crystallization in tellurite glasses," J. Therm. Anal. Calorim. **106**(2), 613–618 (2011).
37. M. R. Kasaai, S. Lagace, D. Boudreau, E. Forster, B. Muller, and S. L. Chin, "Creation of micro-holes on glass surface by femtosecond laser through the ejection of molten material," J. Non-Cryst. Solids **292**(1-3), 202–209 (2001).
38. C. Carteret and A. Labrosse, "Vibrational properties of polysiloxanes from dimer to oligomers and polymers, Structural and vibrational properties of hexamethyldisiloxane $(CH3)_3SiOSi (CH_3)_3$," J. Raman Spectrosc. **41**(9), 996–1004 (2010).
39. M. Schmitt, "Analysis of silanes and of siloxanes formation by Raman spectroscopy," RSC Advances **4**(4), 1907–1917 (2014).
40. M. Mazzuca, J. Portier, B. Tanguy, F. Romain, A. Fadli, and S. Turrell, "Raman scattering in tellurium-metal oxyde glasses," J. Mol. Struct. **349**, 413–416 (1995).
41. T. Komatsu, H. Tawarayama, H. Mohri, and K. Matusita, "Properties and crystallization behaviors of TeO_2LiNbO_3 glasses," J. Non-Cryst. Solids **135**(2–3), 105–113 (1991).
42. K. A. Alim, V. A. Fonoberov, M. Shamsa, and A. A. Balandin, "Micro-Raman investigation of optical phonons in ZnO nanocrystals," J. Appl. Phys. **97**(12), 124313 (2005).
43. D. Yan, P. Wu, S. P. Zhang, L. Liang, F. Yang, Y. L. Pei, and S. Chen, "Assignments of the Raman modes of monoclinic erbium oxide," J. Appl. Phys. **114**(19), 193502 (2013).
44. Y. Jinqiu, C. Lei, H. Huaqiang, Y. Shihong, H. Yunsheng, and W. Hao, "Raman spectra of RE_2O_3 (RE = Eu, Gd, Dy, Ho, Er, Tm, Yb, Lu, Sc and Y): laser-excited luminescence and trace impurity analysis," J. Rare Earths **32**(1), 1–4 (2014).

1. Introduction

For the past two decades, several polymer materials such as siloxanes, poly-methyl methacrylates (PMMA), polyimides, acrylates, and olefins resin have been investigated for optical waveguide engineering, ultrafast optical communications, and optical sensing applications [1–4]. Siloxane-based polymers are cost-effective hybrid organic-inorganic materials predominantly consisting of a silicon and oxygen crosslinked network [3], with remarkable thermal, mechanical and optical properties. In particular, they exhibit excellent thermal stability up to at least 300°C prohibiting the yellowing effects that are commonly observed in polymer materials when exposed to temperatures > 100°C. Additionally, they exhibit low absorption in the near-infrared and visible wavelength range, offer good control of its refractive index, and allow direct fabrication onto various rigid or flexible substrates (Si, glass, FR4, polyimidies) [5–8]. As a result, they have been used extensively in recent years to fabricate optical waveguides directly on printed circuit boards and enable the formation of low-cost optical backplanes and board-level optical interconnects [9–12]. However, the waveguides and waveguide components used in such integrated optical circuits are all passive as currently no suitable on-board optical amplification scheme has been demonstrated. The formation of waveguide amplifiers suitable for use in such applications is a major advance that would eliminate the need for optical-to-electrical conversion and electronic amplifiers and enable more sophisticated all-optical interconnections. In this work therefore, we present work towards this goal by developing a method to efficiently integrate Er-doped glass NPs in siloxane polymer films.

Doping polymer materials with rare earth ions has been studied extensively in recent years due to the potential of producing low-cost waveguide amplifiers. The use of polymer matrices modified with Er^{3+} ions NPs can provide enough isolation between neighbouring ions, and therefore can offer significant improvements in pumping efficiency. Some examples of recent

studies on such rare-earth-modified polymer materials are reported below. Kumar et al. [13] reported on the fabrication and optical properties of CaF: Er^{3+} nanocrystals doped into a perfluorocyobutyl-based fluoropolymer composite. A maximum optical gain of 1.78 dB/cm at the 1560 nm wavelength that corresponds to the Er^{3+} ion transition was obtained. Similarly, the synthesis and fluorescence properties of an Er-doped organic polydentate cage complex has been reported by Sloff et al. [14]. A FWHM of about 70 nm and a lifetime of 0.8 µs were demonstrated from these composite materials. The paper suggests that the decreased lifetime is due to fluorescence quenching induced by the C-H and O–H groups in the organic polydentate. In addition, various groups have tried to synthesize $NaFY_4$:Er^{3+}: Yb^{3+} NPs in PMMA covalent-linking nanocomposites and $NaFY_4$:Er^{3+},Yb^{3+}, Ce^{3+} nanocrystals targeting the formation of polymer-based optical waveguide amplifiers [15-16]. In [15] for example, Zhang et al. synthesized $NaYF_4$/$NaLuF_4$: Yb^{3+},Er^{3+} NPs-PMMA covalent-linking nanocomposites with an optimal concentration ratio of Er^{3+} to Yb^{3+} of 1:10, and demonstrated a net gain of 15.1 dB for a waveguide length of 1.3 cm at 1530 nm. Furthermore, Er^{3+}-doped tellurite glass-polymer superlattice nanolayers have been produced with nanosecond-pulsed laser deposition (ns-PLD) using a 193-nm ultraviolet laser [17]. The PL spectrum of the samples produced showed a FWHM value of 64 nm and a decay lifetime of 1.8 ms at the Er^{3+}: $^4I_{13/2} \rightarrow {}^4I_{15/2}$ transition centred at 1534 nm. Recently, Ghatrehsamani et al. using modelling studies predicted an optical gain of ~15 dB at 1540 nm for an 8 mm long polymer waveguide doped with P_2O_2: Er^{3+}/Yb^{3+} NPs of 10 nm radius [18]. These results and the related intensive research clearly demonstrate that hybrid glass-organic/inorganic nanoparticle thin films are promising candidates for developing high gain Er^{3+}-doped polymer-based optical waveguide amplifiers.

Several fabrication techniques including sol-gel deposition [19], spin coating [20], sputtering [21], ball milling [22], and ion implantation [23] have been employed to synthesize the inorganic active NPs materials and dope the polymer materials. ns-PLD is a particularly promising method as it allows the production of NPs of different sizes, morphology, and chemical composition by adjusting the laser parameters and chamber conditions. It has been utilized to deposit PMMA, polystyrene, and Er^{3+}-doped tellurite glass on polymer thin films [1,17]. In recent years, PLD with even shorter pulse duration in the femtosecond range (fs-PLD) has been used to synthesize NPs from several materials such as chromium, stainless steel, indium [24], aluminium [25], and gold (Au) [26]. Through systematic fabrication studies, it has been demonstrated that fs-PLD is more efficient than ns-PLD in generating NPs with equivalent size distributions and preventing NP agglomeration [27]. Additionally, the fs-PLD technique enables the generation of a wider range of NPs sizes by adjusting the energy of the laser pulses and can provide higher doping concentrations without major fluorescence and lifetime quenching [28]. Furthermore, theoretical models have shown that rapid expansion and cooling of the particles ejected from the target by the femtosecond laser could create NPs through various processes such as heterogeneous decomposition, liquid phase ejection and fragmentation, and homogenous nucleation and decomposition [29]. The formation of NPs by using fs-laser is attractive due to the following reasons as compared to nanosecond laser. Firstly, the ejected material does not interact with the subsequent trace of the fs-laser beam, as in the case of ns-laser deposition which then allow the formation of NPs without any external influence. Secondly, the laser-material interactions generate a lot of heat on the target surface without modifying the optical properties of the material, and as a result, the NPs created retain the either amorphous or crystalline property of the target (if the ejected particles size radii are within 1-1000 nm range). However, in the nanosecond region, the size distribution of the NPs becomes broader and clustered, which is disadvantageous for optical sensing and waveguide applications [30]. The ability to embed rare earth doped nanoparticles within a polymer film is the unique feature of fs-PLD used in this study.

To date, there have been numerous reports of the use of tellurite glasses for the formation of Er-doped waveguide amplifiers [31–33]. Such glasses offer high solubility of rare-earth

ions, and exhibit a broad and strong PL emission at 1534 nm and high amplification gain. For instance, an Er-doped tellurite waveguide has been demonstrated achieving a high gain of 2.8 dB/cm when pumped at 1480 nm [33]. The fabrication of other tellurite-based glass waveguides had been also reported such as TeO_2-WO_3-Na_2O-Er_2O_3 [32] and TeO_2-GeO_2-Na_2O-ZnO-Er_2O_3 [33] with good results. The integration however of Er-doped tellurite NPs with polymer materials is not straightforward as inorganic salts are not readily soluble in polymers and exhibit large difference in thermal expansion coefficient with common polymer materials [34]. To address this issue, we propose here a new approach of incorporating Er^{3+}-TZN glass NPs into polymer materials using fs-PLD. The method allows the efficient formation and embedding of NPs with sizes smaller than 40 nm in the polymer layers achieving a high surface area-to-volume ratio and good film uniformity. To the best of our knowledge, this is the first report of the use of fs-PLD for doping siloxane materials with Er^{3+}- TZN glass NPs. The characterisation of the fabricated Er-doped polymer films provide promising results and indicate good potential for the formation of hybrid glass-polymer waveguide amplifiers. The structure of the remainder of the paper is as follows. Section 2 presents the sample fabrication and the employed characterization techniques while section 3 describes the obtained results. Finally, section 4 provides the conclusions.

2. Experiment

TeO_2-ZnO-NaO_2-Er_2O_3 (Er-TZN) glass NPs are embedded into siloxane polymer films fabricated on silica substrates. The glass NPs are synthesized in a stainless-steel high vacuum chamber using a fs-PLD system. The Er-TZN glass target is synthesized using the conventional melting and quenching technique with a nominal composition of 79.5TeO_2-10ZnO-10NaO_2 + 0.50 Er_2O_3 (in wt.%). The polymer material employed in this work is the Dow Corning Corporation WG-2020 Optical Elastomer. The polymer material is loaded with toluene to reduce the material viscosity and generate films of appropriate thickness using spin coating. The solution is spin-coated onto a silica substrate at 2000 rpm for 1 minute, UV-exposed and hard-baked. The target and polymer-coated silica (PoS) substrates are mounted in the target and substrate holders respectively inside the chamber. The chamber is initially pumped down to $5x10^{-5}$ Torr to avoid contamination and remove any residual water vapour and is then refilled with high purity oxygen with a background pressure of 70 mTorr. The fs laser system employed in the PLD process consists of an amplified Ti: sapphire laser producing 100 fs pulses at an 800 nm wavelength with a variable repetition rate in the range of 0.25 to 1 KHz. The laser output beam is focused onto the target surface at an angle of 60° whilst the target is rotated and rasterised during deposition in order to maintain a constant active target surface elevation. As a result, a steady laser beam spot size and fluence is maintained throughout the deposition process. A laser repetition rate of 0.5 KHz and a target-to-substrate distance of ~60 mm are used during the fabrication of the samples. The substrate temperature is maintained at 100°C, while the laser ablation is performed at two pulse energies: 45 μJ (sample I) and 60 μJ (sample II). The deposition time for these samples is 45 minutes to ensure deposition of adequate NPs for initial characterisation tests.

The surface morphology and transmission electron microscopy (TEM) cross-section of the samples prepared is characterized using high-resolution monochromated field emission scanning electron microscope (FEGSEM) with precise focused ion beam (FIB) (FEI Helios G4 CX DualBeam). The scanning (S)/TEM specimen imaging, and diffraction of the produced glassy-polymer thin film are analysed using high-resolution transmission electron microscopy (HRTEM) (FEI Tecnai F20 200 kV FEGTEM), while the composition of the generated NPs is characterized using energy-dispersive X-Ray spectroscopy. X-ray diffraction (XRD) patterns are measured with a Philips PANalytical X'pert Diffractometer, using Cu Kα radiation (λ = 1.54056 Å), at 40 kV and 100 mA; the diffractometer angle is varied between 3° and 70° with a step size of 0.02°. The photoluminescence spectrum and lifetime measurements are carried out using a FS920 spectrometer (Edinburgh Instruments,

UK). The thin film samples are excited with a semiconductor laser diode emitting at 980 nm. The transmission spectrum is obtained using a Perkin Elmer UV/VIS/NIR Lambda 950 spectrometer operating in the range of 350 to 2000 nm. The vibrational spectrum of Er-doped polymer samples is obtained with the Renishaw Raman microscope under a 514.5 nm laser excitation in the wavenumber range of 200 to 3200 cm^{-1}.

3. Results and discussion

3.1 Surface and morphology of hybrid polymer with erbium-based nanoparticles

Figure 1 shows SEM images of the Er-TZN glass NPs deposited on the surface of the siloxane-coated silica substrates at the 45 µJ (sample I) and 60 µJ (sample II) energies. The purpose of these images focusses on distribution of the NPs into the polymer layer with almost identical particle sizes. It can be observed that the NPs are quite homogeneous across the entire substrate surface in Fig. 1(a). In the case of sample (II), the NPs are well separated from each other. This paper focusses on the applicability of the fs-PLD for the formation of glass-polymer composite films and reports on the basic studies on-their interface properties

Further analysis of the SEM images with ParticleMetric software and then verified by ImageJ, the sample II reveals large number of NPs dispersed into polymer layer with irregular shape, while their size ranges from 15 to 37 nm. Their average size is estimated to be ~21 nm. On the other hand, sample I which is fabricated at the lower energy of 45 µJ shows significantly smaller particles with spherical morphology and an average particle size of ~11 nm.
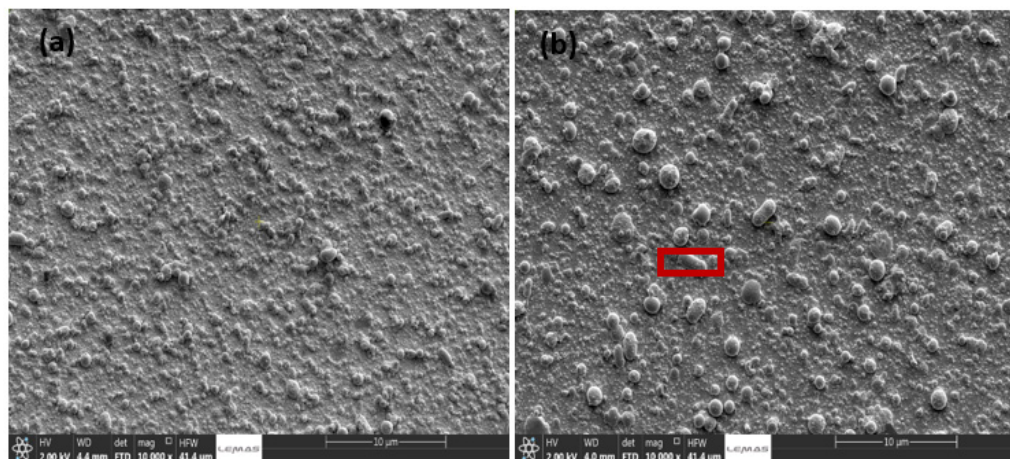

Fig. 1. SEM images of the Er-TZN glass NPs deposited on siloxane polymer-coated silica substrate at (a) 45 µJ (sample I) and (b) 60 µJ (sample II).

Figure 2 shows the FIB cross-section that is milled out from the marked region in Fig. 1(b) and is used for TEM imaging, as well as the selected area electron diffraction (SAED) patterns obtained from a representative Er-TZN glass NPs in the samples. The existence of spherical overlap rings around the central spot (marked 22 & 27 in Fig. 2) and broad diffuse (marked 21 in Fig. 2(a)) ring regions of the hybrid polymer-glass NPs thin film in the SAED pattern confirms the presence of the nanocrystallite and amorphous regions within the particle. The silica substrate exhibits broad diffuse rings for non-crystalline materials which agrees with its amorphous nature. Similar observations are made on the Er-TZN glass NPs incorporated into sample I. It should be pointed out that during deposition, once the laser fluence is increased slightly above the breakdown threshold of the target, the temperature in the interaction region increases [35], which can induce a complete or partial phase transition of the material from amorphous to nanocrystallite phase. In addition to this, fast cooling of

the ejected particles from the target to the substrate (due to the substrate temperature) decreases the number of particles and the growth rate, which favours build-up of fast atoms as well as crystalline nanoparticles. The nanocrystallite observed in the SAED patterns can be attributed to the formation of α-TeO$_2$ (paratellurite) and δ-TeO$_2$ (tellurite) crystalline phases [36]. The plan-view of TEM measurements reveals an average film thickness of around 43.17 and 45.47 nm for samples I and II respectively.
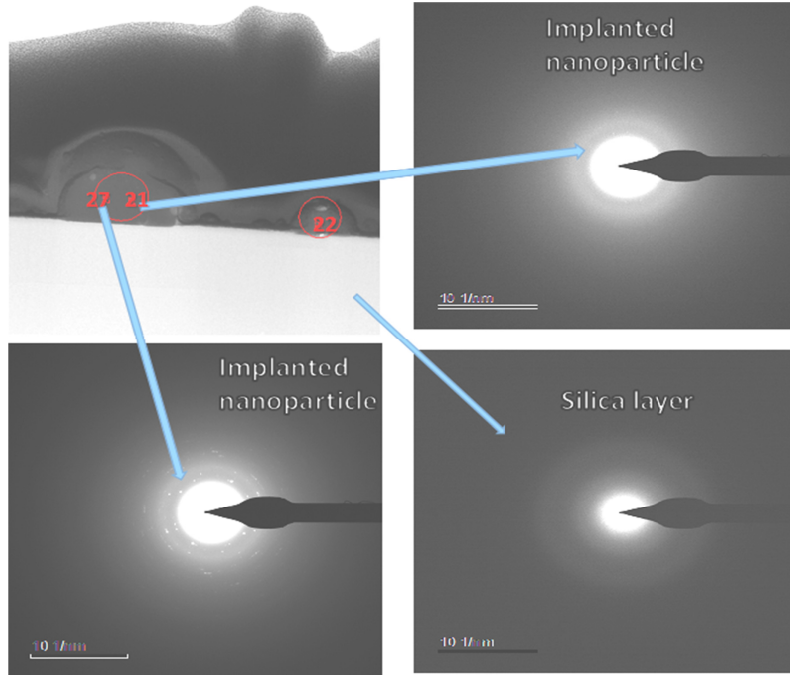
Fig. 2. HRTEM image of the interface between silica matrix and the siloxane polymer-coated silica substrate modified Er-TZN glass NPs (upper left); and SAED patterns on the bottom and right hand side at 60 µJ (sample II).
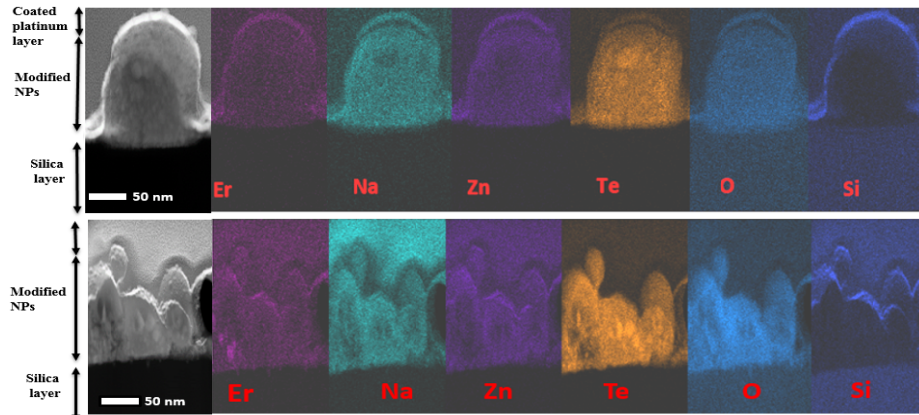
Fig. 3. EDX-SEM chemical mapping acquired during cross-sectional STEM analysis from the rectangular regions in Fig. 1(a) and (b) indicating the elemental distribution of erbium (Er), sodium (Na), zinc (Zn), tellurium (Te), oxygen (O), and silicon (Si) which comprises of polymer layer.

Figure 3 shows the cross-sectional elemental map of the siloxane layer modified with Er-TZN glass NPs acquired from sample (I) and sample (II) substrates. The scanning TEM

energy dispersive X-ray (EDX) spectroscopy and chemical mapping clearly show the elemental distribution of erbium, sodium, zinc, tellurium, oxygen, and silicon in the sample. The silicon, only present in the polymer is seen as thin layer over the glass particles. From both Figs. 3(a) and 3(b), it can be confirmed that the nanoparticles or clusters of glass particles are encapsulated within the polymer but without any molecular level intermixing.

Figure 4 shows the XRD patterns obtained from the target glass and fabricated siloxane-coated silica samples modified with Er-TZN glass NPs. The target glass shows two characteristic broad amorphous bands at $2\theta = 28.59°$ and $51.55°$, while the films prepared by the fs-PLD exhibit amorphous silica evolved at $2\theta = 22.5°$. It is important to mention that the size of the particle generated from the target are in nano-sized, therefore, the XRD instrument could not detect the crystalline diffractions phases observed in the SAED analysis of the TEM image shown in Fig. 2. Henceforth, the presence of the crystalline phase in the polymer modified Er-TZN glass NPs could not be completely ruled out using the XRD results. For instance, Kasaai et al. [37] demonstrated the presence of crystallization in the particles irradiated from the surface of a fused silica using a femtosecond laser. However, the XRD results obtained here suggest that the irradiated surface of the fused silica remains amorphous.
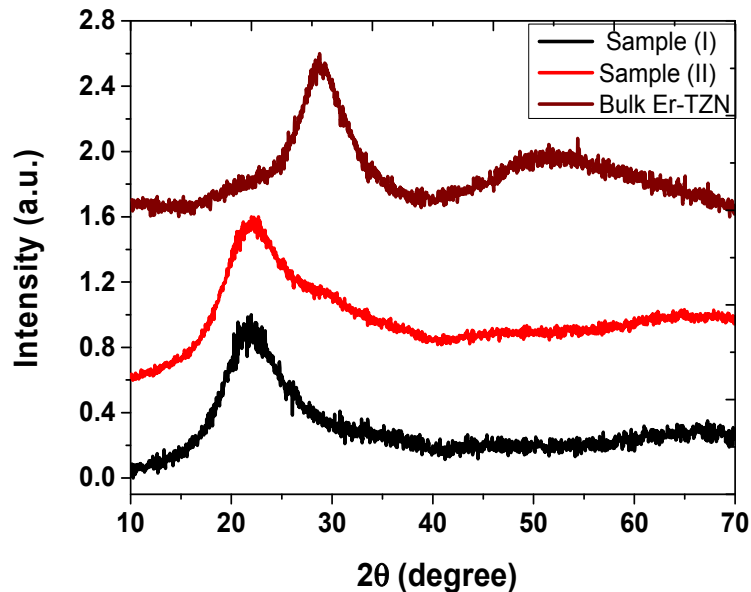

Fig. 4. XRD pattern obtained from the bulk Er-TZN target glass and Er-doped polymer at sample (I) and sample (II).

The Raman spectra of the unmodified polymer thin film and the modified layer with the Er-TZN glass NPs at the two different pulse deposition energies obtained under a 514.5 nm excitation are shown in Fig. 5. The Raman spectra reveal two bands with peaks at 2800 cm^{-1} and 3060 cm^{-1} in all the three samples, which, however, are not observed in the bulk target glass sample. These Raman bands correspond to methyl-group (CH_3) symmetric (V_s) and asymmetric (V_a) stretching vibrations [36]. Also, the Raman spectrum for the unmodified polymer thin film exhibits additional vibration bands centred at ~616, 1126, 1418, and 1600 cm^{-1}. These however, are not detected in the modified polymer layer with the Er-TZN NPs. The peak occurring at 616 cm^{-1} can be assigned to symmetric and asymmetric stretching of $Si(-O-CH_3)_3$ or SiC_3 stretch, while the 3 remaining bands (1126, 1418, and 1600 cm^{-1}) can be attributed to CH_3 symmetrical stretching mode deformation [38, 39]. Moreover, doping the

polymer thin film with Er-TZN NPs yielded additional broad bands that comprised three vibration modes in the 100-480 cm^{-1}, 480-890 cm^{-1}, and 890-1860 cm^{-1} frequency ranges. This clearly shows a noticeable difference between the plain polymer sample (PoS) and the Er-doped polymer samples. According to Mazzuca el at [41], the sharp shoulder identified at 121 cm^{-1} (peak A) is attributed to vibrations due to the TeO_4–ZnO_6–TeO_3 chain structure. The Zn acts as a glass network-forming link, which agrees with $ZnTeO_3$ and $Zn_2Te_3O_8$ crystals vibrational wavenumbers. The Raman shift frequency observed at 281 cm^{-1} (peak B) is assigned to TeO_3 trigonal pyramids (tp) and Er–O bonds [39], whilst the peaks around 355 cm^{-1} (peak C) are attributed to the Zn-O content [40, 42]. The vibration band at 480-890 cm^{-1} which is centred at 620 cm^{-1} (peak D) corresponds to stretching vibration of the metastable or B-Phase Er_2O_3 (B- Er_2O_3) groups, respectively [43]. Following Jinqiu et al. [44], higher vibration bands centred at 1140 and 1420 cm^{-1} (peaks E and F) are ascribed to B-Er_2O_3 bonds, respectively.
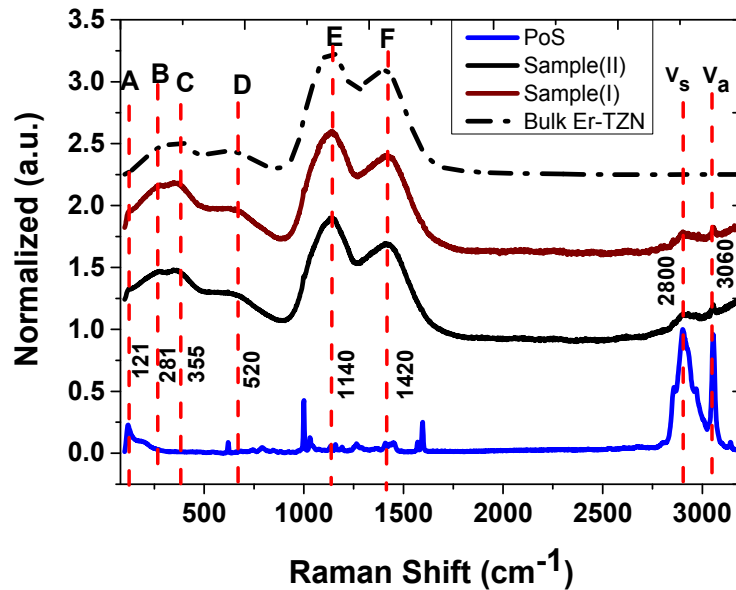

Fig. 5. Raman spectra using 514.5 nm laser as excitation source of bulk sample, polymer coated silica, and modified with Er-TZN NPs at sample (I) and sample (II).

3.2 Optical characteristics of hybrid polymer with erbium-based nanoparticles

Figure 6 shows a comparison of the normalized photoluminescence spectra obtained from the Er-doped polymer samples at room-temperature and the bulk target sample under a 980 nm laser diode excitation. The fluorescence peak centred at 1534 nm is assigned to the transition from the first excited state ($^4I_{13/2}$) to the ground state ($^4I_{15/2}$) of the Er^{3+} ions. The figure clearly exhibits a broad and intense band for the bulk glass sample with a FWHM of 51 nm. For the fabricated samples, the FWHM of the central 1534 nm peak was reduced to 39.2 nm. The fluorescence lifetime of the target and fabricated samples were measured around 1534 nm ($^4I_{13/2}$ transition) using the same 980 nm excitation. The experimental data was fitted with a single exponential function and lifetime values of 4.37, 3.52, and 4.18 ms were obtained for the bulk target material and modified polymer layer samples prepared at 45 and 60 µJ respectively. A minor drop in the lifetimes of the Er-TZN glass NPs incorporated into polymer layer when compared to that of the target glass is observed and this can be attributed

to fluorescence quenching induced by the C-H phonon vibration bonds in the polymer centred at 2800 cm^{-1} and 3060 cm^{-1}.
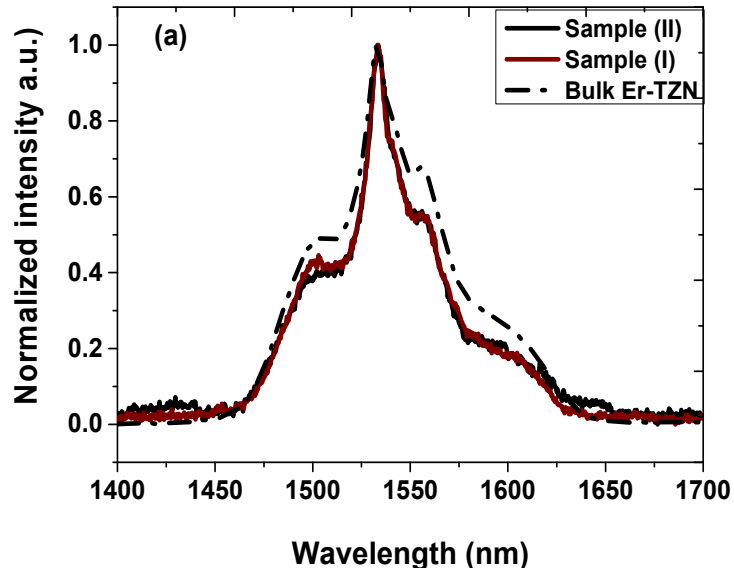

Fig. 6. Normalized photoluminescence spectra of bulk Er-TZN target glass, and polymer modified with Er-TZN NPs (sample (I) and sample (II)) at room temperature via 980 nm continue wave (cw) excitation source.

   The optical transmission spectra of the unmodified polymer-coated silica and samples prepared at 45 µJ (sample I) and 60 µJ (sample II) energies are shown in Fig. 7. The transmission of the unmodified polymer-coated silica is ~90% in the 400-2000 nm wavelength range indicating good transparency. The transmission of sample I is found to be between 75 and 90% within the same wavelength range, while sample II exhibits a reduced transmission with values ~85% at 2000 nm. This is expected due to the larger number of glass NPs deposited onto the polymer film at higher energies.
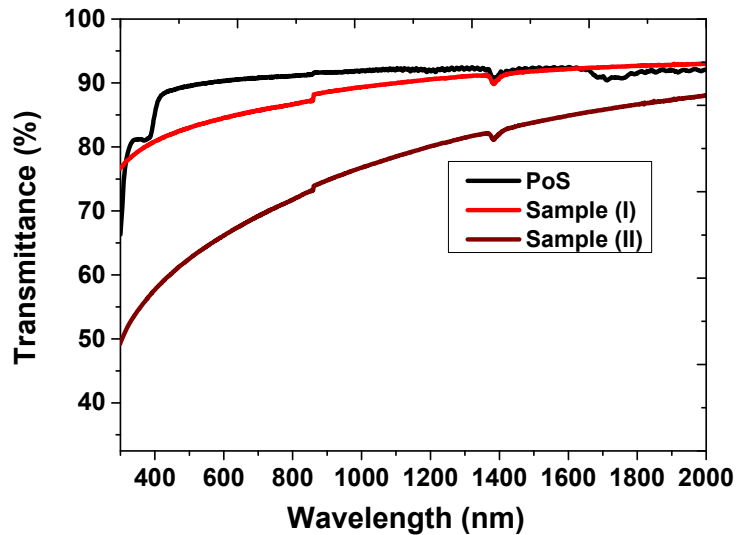
Fig. 7. Transmittance of plain polymer-coated silica samples and samples modified with Er-TZN NPs glass processed for sample (I) and sample (II).

4. Conclusions

In this work, we present a novel technique to deposit Er-TZN glass NPs on polymer films using fs-PLD. The evaluation of the morphological, compositional and structural characteristics of the Er-TZN glass NPs deposited in the polymer layer does not indicate any significant structural modification of the NPs when compared with the properties of the target material. The SEM images and FIB-TEM measurements reveal the dependence of the size of the deposited NPs and thickness of the produced glass film on the laser pulse energy. Hybrid polymer-Er-TZN glass NPs embedded polymer films are fabricated using this method. A PL FWHM of 39 nm and an Er lifetime in the range of 3.52 to 4.18 ms are obtained under 980-nm laser excitation. Although some differences in the obtained FWHM and Er lifetime values are observed between the fabricated samples and the bulk target material, the obtained results are promising for the formation of hybrid optical waveguide amplifiers and sensing.